Structure
Article

Structural Model and *trans*-Interaction of the Entire Ectodomain of the Olfactory Cell Adhesion Molecule

Nikolaj Kulahin,[1,2,3,4] Ole Kristensen,[2] Kim K. Rasmussen,[1,2] Lars Olsen,[2] Patrik Rydberg,[2] Bente Vestergaard,[2] Jette S. Kastrup,[2] Vladimir Berezin,[1] Elisabeth Bock,[1] Peter S. Walmod,[1,*] and Michael Gajhede[2,*]
[1]Protein Laboratory, Department of Neuroscience and Pharmacology, Faculty of Health Sciences, University of Copenhagen, DK-2200 Copenhagen N, Denmark
[2]Biostructural Research, Department of Medicinal Chemistry, Faculty of Pharmaceutical Sciences, University of Copenhagen, DK-2100 Copenhagen O, Denmark
[3]ENKAM Pharmaceuticals A/S, DK-2100 Copenhagen O, Denmark
[4]Present address: Receptor Systems Biology Laboratory, Hagedorn Research Institute, DK-2820 Gentofte, Denmark
*Correspondence: psw@sund.ku.dk (P.S.W.), mig@farma.ku.dk (M.G.)
DOI 10.1016/j.str.2010.12.014

SUMMARY

The ectodomain of olfactory cell adhesion molecule (OCAM/NCAM2/RNCAM) consists of five immunoglobulin (Ig) domains (IgI–V), followed by two fibronectin-type 3 (Fn3) domains (Fn3I–II). A complete structural model of the entire ectodomain of human OCAM has been assembled from crystal structures of six recombinant proteins corresponding to different regions of the ectodomain. The model is the longest experimentally based composite structural model of an entire IgCAM ectodomain. It displays an essentially linear arrangement of IgI–V, followed by bends between IgV and Fn3I and between Fn3I and Fn3II. Proteins containing IgI–IgII domains formed stable homodimers in solution and in crystals. Dimerization could be disrupted in vitro by mutations in the dimer interface region. In conjunction with the bent ectodomain conformation, which can position IgI–V parallel with the cell surface, the IgI–IgII dimerization enables OCAM-mediated *trans*-interactions with an intercellular distance of about 20 nm, which is consistent with that observed in synapses.

INTRODUCTION

Neural cell adhesion molecules (CAMs) have adhesive properties that are of major importance for the self-assembly of interconnections between cells in the mammalian brain. Additionally, they have many other functions related to cell-cell signaling (reviewed in Shapiro et al., 2007). CAMs are divided into several families, including the integrins, selectins, cadherins, and CAMs of the immunoglobulin (Ig) superfamily (Juliano, 2002). CAMs are generally multidomain proteins with the extracellular part comprising domains in a modular arrangement. The molecular mechanisms controlling the various functions of CAMs have attracted much attention from the field of drug discovery. For example, CAMs can be essential therapeutic targets for the treatment of cancer or neurodegenerative diseases (Raveh et al., 2009; Rice et al., 2005).

Mammalian forms of olfactory cell adhesion molecule (OCAM/NCAM2/RNCAM) were cloned in 1997 (Alenius and Bohm, 1997; Paoloni-Giacobino et al., 1997; Yoshihara et al., 1997). OCAM exists in a transmembrane and a glycosylphosphatidylinositol-anchored isoform resulting from alternative splicing of the transcript from a single gene (reviewed in Kulahin and Walmod, 2010). OCAM transcripts are found in several tissues (Paoloni-Giacobino et al., 1997) including different regions of the brain where it is believed to regulate neurite outgrowth, axonal guidance, synapse formation, and the formation of dendritic bundles (Hamlin et al., 2004; Ichinohe et al., 2003; Paoloni-Giacobino et al., 1997). The expression of OCAM has been suggested to potentially influence certain types of neurological diseases, including autism (Molloy et al., 2005) and Down's syndrome (Paoloni-Giacobino et al., 1997), and studies also indicate that the expression of OCAM can be changed in, for example, prostate cancer cells (Edwards et al., 2005; Xu et al., 2001).

OCAM is a paralog of neural cell adhesion molecule 1 (NCAM1) (see Owczarek et al., 2009), and the extracellular part of both proteins consists of five N-terminal Ig domains (IgI–V), followed by two fibronectin type III domains (Fn3I–II) (Figure 1). Cell aggregation studies have shown that OCAM mediates homophilic *trans*-interactions, but the domains involved in the interaction have not been identified. Additionally, in vitro binding assays suggest that OCAM does not participate in heterophilic interactions with NCAM1 (Yoshihara et al., 1997).

The molecular basis for homophilic interactions within the IgCAMs has been investigated in, for example, the L1CAM family (Haspel and Grumet, 2003) and DSCAM (Sawaya et al., 2008). Within the NCAM family, the crystal structures of the N-terminal Ig domains IgI–II (Kasper et al., 2000) and IgI–III (Soroka et al., 2003) of NCAM1 have been determined (reviewed in Soroka et al., 2010), and recently, the crystal structure of OCAM Ig1 was published (Rasmussen et al., 2008).

Structural models of the entire ectodomain only exist for relatively short IgCAMs, such as P0 (one Ig domain), JAM1 (two Ig

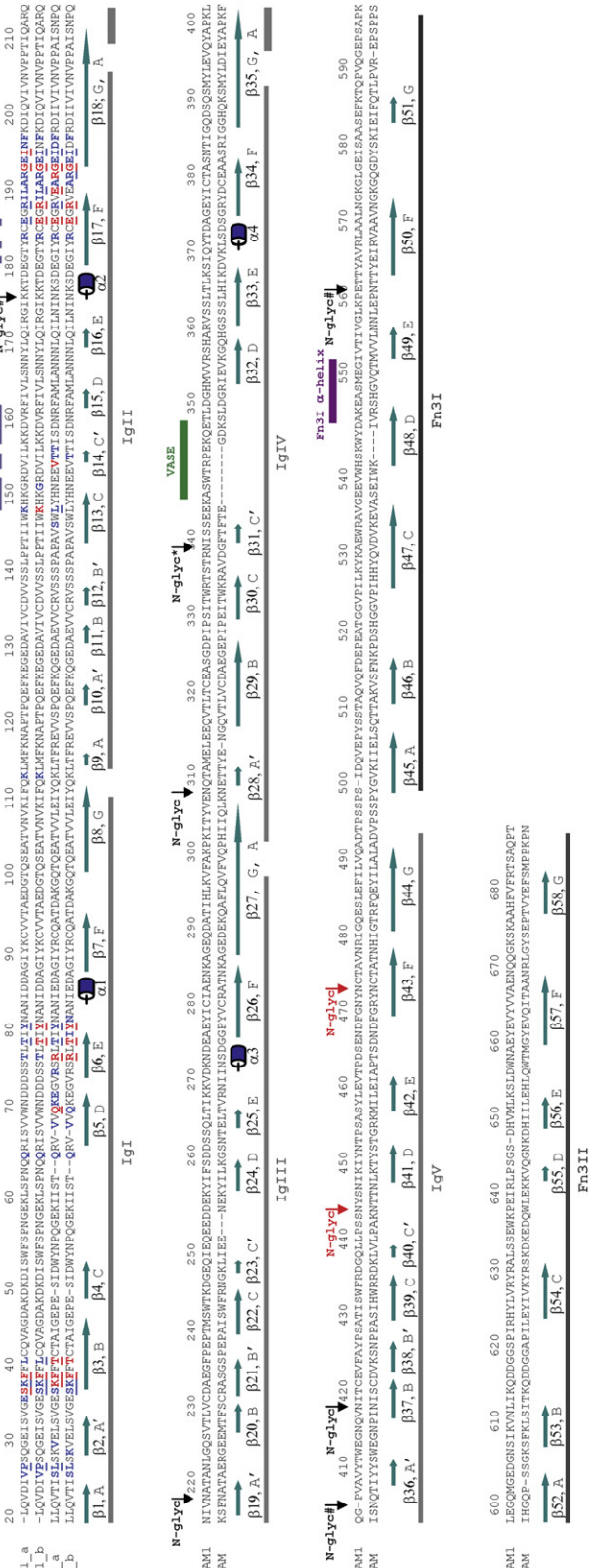

Figure 1. Alignment of NCAM1 and OCAM Ectodomains

NCAM1_a, NCAM1_b, OCAM_a, and OCAM_b correspond to the crystal structures of NCAM1 IgI–II (PDB code 1epf), NCAM1 IgI-III (PDB code 1qz1), OCAM IgI-II (PDB code 2XY2), and OCAM IgI-III (PDB code 2wim), respectively. The assignment of OCAM secondary-structure elements using the dssp program (Kabsch and Sander, 1983) is shown below the sequences. Residue numeration is shown for OCAM (Uniprot code O15394) above the sequences. Residues involved in IgI–II dimer formation are colored blue or red. Residues that are involved in IgI–II/IgI–II dimer formation and in making hydrogen bonds or salt bridges are colored red. Furthermore, residues that are buried more than 50% in the interface are underlined. Residues proposed to be involved in the dimerization include residues giving positive contribution to the interaction energy as defined in the PISA software (http://www.ebi.ac.uk/msd-srv/prot_int/cgi-bin/piserver). N-linked glycosylation sites are marked as N-glyc (present in both NCAM1 and OCAM), N-glyc* (present only in NCAM1), and N-glyc# (present only in OCAM). N-linked glycosylation sites polysialylated in NCAM1 IgV are marked as N-glyc and colored red. HBS indicates the heparin-binding site in NCAM1 IgII (Lys152-Arg156, Val158, Ile159, Lys161-Phe166, Gly185, Tyr187, and Glu190 in NCAM1; Uniprot code P13591). VASE indicates the region in NCAM1 IgIV encoded by the VASE exon, and Fn3I α helix indicates the α helix in NCAM1 Fn3I essential for IgV polysialylation.

domains), and SIRPα (three Ig domains) (Hatherley et al., 2009; Prota et al., 2003; Shapiro et al., 1996). For longer IgCAMs, structures of ectodomain segments are available for TAG-1 (four out of ten extracellular domains) and DSCAM (eight out of 16 extracellular domains) (Mortl et al., 2007; Sawaya et al., 2008). However, no structural models of the entire ectodomain of long IgCAMs have been proposed.

Here, we present a structural model of the entire ~700 amino acid-long ectodomain of human OCAM, assembled from crystal structures of six recombinant proteins with overlapping primary sequences. This represents the longest experimentally based composite structural model of the entire extracellular part of an IgCAM. The ectodomain forms homodimers via the membrane-distal IgI and IgII domains, resulting in a model for OCAM-mediated cell-cell adhesion with an intercellular distance of ~20 nm.

RESULTS

Crystal Structures of the Extracellular Domains of OCAM

The crystal structures of recombinant proteins corresponding to the IgI–II, IgII–III, IgI–III, IgIII–IV, IgIV–F3I, and IgIV–F3II domains of human OCAM have been determined (Figures 2–4 and Table 1). The structures of IgI, IgII, and IgIII all fall into the intermediate 1 (I1) subset of Ig domains (Wang and Springer, 1998). Overall, these three domains are structurally similar to those of NCAM1, with root-mean-square deviations (rmsds) on Cα atoms ranging from 0.6 to 0.9 Å. However, important differences exist between the structures of the Ig domains from NCAM1 and OCAM. A C′ strand that is present in OCAM IgII (Figures 1 and 3) is missing in the corresponding NCAM1 IgII region, a region known to be involved in heparin binding (Kulahin et al., 2005b; Nielsen et al., 2010; Reyes et al., 1990). Consequently, the heparin-binding site of NCAM1 is not conserved between the two proteins (Figure 1). Moreover, the conformations of the loop regions corresponding to the NCAM1 heparin-binding sequence are very different between NCAM1 and OCAM, and

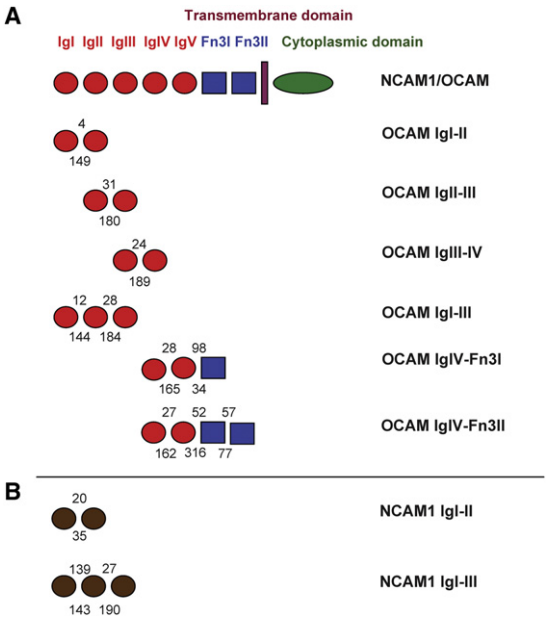

Figure 2. Overview of NCAM1 and OCAM Structures

(A) Schematic representation of NCAM1 and OCAM organization and of recombinant OCAM proteins presented in this study. Tilt/twist angles are shown above/below the constructs. The interdomain geometry was determined according to Bork et al. (1996). The tilt and twist angles were determined by calculating planes through the β strands in each domain, and the z axis was defined as passing along the long axis of the molecule. Corresponding β strands in the Ig domains in question were superimposed on each other, and the angle of rotation around the z axis required to superimpose the calculated planes of the domains was defined as the twist angle. The tilt angle was defined as the angle between the z axes of the two domains.

(B) Schematic representation of NCAM1 IgI-II (PDB code 1epf) and IgI–III (PDB code 1qz1) domains with tilt/twist angles shown above/below the constructs.

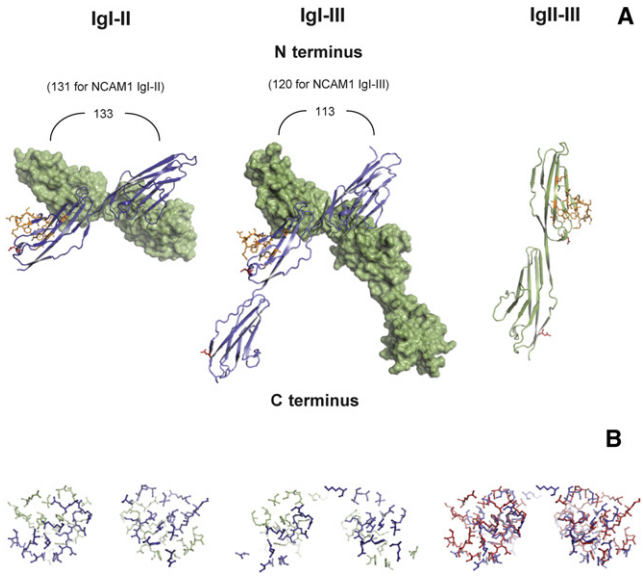

Figure 3. Structures of Recombinant OCAM IgI–II, IgI–III, and IgII–III

(A) Structures of recombinant OCAM IgI–II (PDB code 2XY2), IgI–III (PDB code 2wim), and IgII–III (PDB code 2v5t) with the intermolecular IgI–II angles indicated. The corresponding angles in NCAM1 structures are given in parentheses. N-linked glycosylation sites are shown as sticks and colored red. Residues of the IgII domain of OCAM, corresponding to the heparin-binding site in NCAM1 (Lys152-Arg156, Val158, Ile159, Lys161-Phe166, Gly185, Tyr187, Glu190 in NCAM1; Uniprot code P13591), are shown as sticks and colored orange.

(B) IgI–II dimer interfaces. The IgI–II dimer interface in the IgI–II structure is shown on the left (with two monomers colored in green and blue, respectively); the IgI–II dimer interface in the IgI–III structure is shown in the middle (with two monomers colored in green and blue, respectively). On the right, the two dimer interfaces are superimposed with the IgI–II dimer interface derived from the IgI–II in red and the dimer interface from the IgI–III structure in blue. See also Figures S1, S3, and S4, and Tables S1 and S2.

because the residues Glu153 and Glu154 (Uniprot code O15394) are disordered in the OCAM IgI–II, IgII–III, and IgI–III structures, this region may be more flexible in OCAM than in NCAM1.

The loop connecting the IgIII C and D strands is three residues shorter in OCAM than in NCAM1. Whereas this loop is disordered in the NCAM1 IgI–III structure, it is clearly defined in the OCAM IgI–III, IgII–III, and IgIII–IV structures. This ordering may be related to the hydrogen bond formed between Tyr257 N and Asn254 O. Notably, OCAM IgIV appears to belong to the variable (V) subset of Ig domains due to the presence of a putative C″ strand. However, whereas the C″ strand is well defined in the IgIII–IV structure, it is disordered in the IgIV–Fn3I and IgIV–Fn3II structures. The loop region 346-GDKS-349 is one of the most flexible regions in IgIV, and it is disordered in the OCAM IgIV–Fn3I and IgIV–Fn3II structures. This loop corresponds to the sequence in NCAM1 IgIV encoded by the VASE mini-exon (354-ASWTRPEKQE-363) (Figure 1), which in NCAM1 is associated with downregulated neural plasticity (reviewed in Owczarek et al., 2009). The IgV structure is most closely related to the OCAM IgIII structure, with a Z-score of 13.1 and an rmsd of 1.9 Å using the DALI server (Holm et al., 2008), thus placing it in the I1 subset of the Ig domains.

A DALI search revealed that the OCAM Fn3I structure is most closely related to the NMR structure of the same domain (PDB code 2doc), with an rmsd of 0.8 Å. It is also very similar to Fn3I and Fn3II of NCAM1 (Carafoli et al., 2008; Kiselyov et al., 2003; Mendiratta et al., 2006), with rmsds of 1.1 and 1.2 Å, respectively. The structure of OCAM Fn3II is most similar to the NMR structure of the same domain (PDB code 2kbg), with an rmsd of 1.1 Å.

Glycosylation of OCAM

Human OCAM contains eight potential sites for N-linked glycosylation, five of which are also found in NCAM1 (Figures 1 and 5). However, in contrast to NCAM1, OCAM has been reported not to be glycosylated with the unusual carbohydrate polysialic acid (PSA; long, negatively charged homopolymer of α2-8-*N* acetylneuraminic acid). N-linked glycosylation was clearly visible at Asn177 in IgII, Asn219 in IgIII, Asn309 in IgIV, and Asn419, Asn445, and Asn474 in IgV and could be unambiguously fitted into the electron densities. The Asn177 glycosylation site is absent in NCAM1, due to the presence of lysine at this position. Glycosylation sites Asn445 and Asn474 in OCAM IgV, corresponding to the polysialylation sites in NCAM1, are shown in Figures 1, 4, and 5. Notably, the α helix between strands D and E in the NCAM1 Fn3I domain (562-AKEASMEG-569; Figure 1),

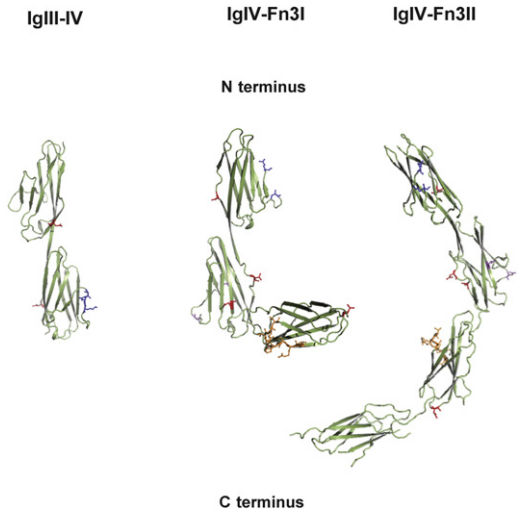

Figure 4. Structures of Recombinant OCAM IgIII–IV (PDB Code 2XY1), IgIV–Fn3I (PDB Code 2XYC), and IgIV–Fn3II (PDB Code 2jII)
N-linked glycosylation sites are shown as sticks and colored red. OCAM residues polysialylated in NCAM1 are shown in purple, and the region in OCAM Fn3I, corresponding to the α helix in NCAM1 critical for polysialylation, is shown in orange. Residues indicating the position of the NCAM1 region encoded by VASE exon are shown in blue. See also Figures S2 and S3, and Tables S1 and S2.

which has been shown to be implicated in polysialylation of the NCAM1 IgV domain (Colley, 2010; Mendiratta et al., 2006), is not present in OCAM, and indeed OCAM has been reported not to be polysialylated (Yoshihara et al., 1997).

Interdomain Arrangements

The link region between OCAM IgI and IgII appears almost linear, with tilt and twist angles of 4°–12° and 144°–149°, respectively (Figure 2A). The most prominent interdomain interaction observed is a hydrophobic stacking of Arg193 and Tyr112. Arg193 also forms hydrogen bonds to the carbonyl oxygen atoms of residues Gln113 and Ser141. Altogether, this arrangement appears to confer rigidity to the linking region between the two domains. A similar stacking interaction is found in the NCAM1 structure, where the corresponding arginine forms an interdomain salt bridge to Glu30 (Uniprot code P13596). With a tilt angle of 28°–31°, IgII and IgIII are positioned in a near-linear arrangement. The conformation is stabilized by interdomain hydrogen bonds and salt bridges. Glu125 forms a salt bridge to Lys286, and the side chain of Lys127 forms a hydrogen bond to the carbonyl oxygen atom of Ala287. The tilt angle in OCAM IgII–III is very similar to that of NCAM1. A salt bridge between OCAM residues Glu125 and Lys127 is also seen in NCAM1 (Glu128 and Lys293). The equivalent of the hydrogen bond between OCAM residues Lys127 and Ala287 is also formed in NCAM1 between Lys130 and Ala294. The OCAM IgIII G strand and the IgIV A strand form one long strand in the structure. Along with the interdomain hydrogen bond formed between residues Arg224 and Gln301, this long strand may stabilize the domain interface at a twist angle of 24°. Similarly, the OCAM IgIV G strand is extended into the IgV domain, where it forms one long β strand together with the A strand of IgV. Many other interdomain interactions between IgIV and IgV are present, including hydrogen bonds between Asp396 and Asn427, Glu398 and His480, and Glu398 and Asn427. The observed tilt angle is 27°–28°, again corresponding to a near-linear arrangement of the domains.

The interdomain link between IgV and Fn3I in the OCAM IgIV–Fn3II structure is more bent than the linker regions between Ig domains, with a tilt angle of 52°. One interdomain hydrogen bond between Trp413 and Gly524 stabilizes the interface. The only other interdomain interaction observed is a hydrophobic stacking of Trp413 and Lys575. IgIV and IgV of the IgIV–Fn3I structure have fold and interdomain link-region interactions that are very similar to those observed in the IgIV–Fn3II structure. However, the IgV–Fn3I link is significantly different in the two structures. The presence of a HEPES molecule appears to play an important role in stabilizing the conformation between IgV and Fn3I in this crystal structure (see Figure S2 available online). The HEPES molecule makes hydrophobic contacts with Tyr411, Ala493, Asp494, Val495, Pro496, Ser497, Ser498, and Val525, and the complex is further stabilized by hydrogen bonds through two water molecules. The observed tilt angle between Fn3I and Fn3II is 57°. When examining the linkage between Fn3I and Fn3II, no hydrogen bonds or other types of interactions are evident.

Molecular dynamics simulations were conducted on a number of recombinant OCAM proteins. Ten-nanosecond simulations on monomeric IgI–III domains showed several large folding and twisting motions around the hinges between the domains. The movements around the IgI–II hinge were significantly larger than the movements around the IgII–III hinge, and the tilt angles of the domains varied from 12° to 73° around the IgI–II hinge (compared with only 28°–44° for the IgII–III hinge) (Table S1).

Two simulations of IgIV–Fn3I with and without the HEPES molecule showed significant differences. The simulation with the HEPES molecule bound to the protein only showed small variations compared with the crystal structure, and the simulation without HEPES displayed significant movement of the domains. During this simulation the tilt angle between the IgV and Fn3I domains changed from 98° (similar to the crystal structure) toward an equilibrium value of 65° (which is close to the tilt angle observed in the IgIV–Fn3II structure). The amino acids Leu395, Asp396, Leu490, Ala491, and Leu492 have been identified (by analysis backbone torsional angle changes) as being primarily responsible for the change in the tilt angle. The difference between the two simulations of IgIV–Fn3I with and without the HEPES molecule indicates flexibility in the IgV–Fn3I linker region and that the HEPES molecule is stabilizing the conformation observed in the crystal structure.

The simulations of the IgIV–Fn3II structure (four domains and three hinges) showed some flexibility of the hinges, with the Fn3I–Fn3II hinge being most flexible. Thus, the tilt angle between IgIV and IgV varied from 24° to 27°, between IgV and Fn3I from 50° to 52°, and between Fn3I and Fn3II from 57° to 82°. During the simulations, no conformations were even remotely similar to the IgIV–Fn3I structure with a HEPES molecule bound. Thus, analysis of the longest recombinant OCAM proteins indicated that most of the flexibility of the OCAM ectodomain originates from the IgI–II hinge.

Table 1. Data Collection and Processing Statistics for OCAM IgI–II, IgII–III, IgI–III, IgIII–IV, IgIV–Fn3I, and IgIV–Fn3II

Construct	OCAM IgI–II	OCAM IgII–III	OCAM IgI–III	OCAM IgIII–IV	OCAM IgIV–F3I	OCAM IgIV–F3II
X-ray source	I911-2, MAX-Lab, Lund, Sweden	ID23-1, ESRF, Grenoble, France	ID29, ESRF, Grenoble, France	ID23-2, ESRF, Grenoble, France	I911-5, MAX-Lab, Lund, Sweden	ID29, ESRF, Grenoble, France
Wavelength (Å)	1.041	0.979	0.976	0.873	0.908	0.976
Space group	$P3_12_1$	$P4_12_12$	$P2_12_12_1$	$P2_1$	$P4_32_12$	C2
Unit-cell parameters						
a (Å)	42.06	114.95	38.39	43.81	139.66	151.74
b (Å)	42.06	114.95	106.78	45.81	139.66	33.80
c (Å)	202.91	46.00	188.74	45.72	47.79	97.67
β (°)	–	–	–	103.58	–	98.36
Resolution (Å)	28.99–1.82 (1.87–1.82)	20.0–2.00 (2.11–2.00)	24.57–3.00 (3.08–3.00)	20.2–1.98 (2.03–1.98)	62.46–2.51 (2.57–2.51)	19.79–2.30 (2.42–2.30)
Number of unique observations	19,558	21,021	15,703	12018	16752	38513
Redundancy	4.6 (4.5)	5.9 (6.1)	4.7 (4.7)	3.7 (3.6)	7.1 (7.2)	3.7 (3.8)
Completeness (%)	99.5 (95.9)	98.7 (98.7)	91.9 (96.1)	96.8 (90.9)	99.9 (100)	90.4 (99.9)
$I/\sigma(I)$	23.1 (3.0)	15.60 (2.80)	16.60 (3.80)	10.40 (2.6)	14.60(2.90)	8.60 (2.30)
R_{sym} (%)[a]	3.5 (50.4)	9 (25)	6 (39)	8.5 (58.9)	10.1 (72.6)	4.2 (27.2)
Refinement						
R_{work} (%)[b]	20.3	18.2	21.3	20.0	19.4	21.6
R_{free} (%)[c]	24.0	23.4	28.7	26.6	24.1	26.9
Total atoms	1,696	1,730	4,283	1,647	2,594	3,241
Protein	1,501	1,458	4,209	1,526	2,339	3,031
Water	175	210	31	93	183	147
Ligands	20	62	43	28	72	63
Rmsd bond lengths (Å)	0.007	0.005	0.006	0.007	0.008	0.004
Rmsd bond angles (°)	1.052	0.732	0.978	1.149	1.157	0.921
Mean B ($Å^2$)	35.3	26.5	96.58		39.7	51.3
Ramachandran plot (%)[d]	92.4; 6.4; 1.2; 0.0	90.0; 10.0; 0.0; 0.0	76.3; 20.8; 2.1; 0.8	91.5; 7.9; 0.6; 0.0	87.4; 11.9; 0.4; 0.4	88.6; 10.5; 0.9; 0.0

Values in parentheses are for the highest resolution shell.

[a] $R_{sym} = \sum_{hkl} (\sum_i |I_{hkl,\,i} - \langle I_{hkl}\rangle|)/\sum_{hkl,\,i} \langle I_{hkl,\,i}\rangle$, where $I_{hkl,\,i}$ is the intensity of an individual measurement of the reflection with Miller indices *h*, *k*, and *l*, and $\langle I_{hkl}\rangle$ is the mean intensity of that reflection.

[b] $R_{work} = \sum_{hkl} (||F_{o,\,hkl}| - |F_{c,\,hkl}||)/|F_{o,\,hkl}|$, where $|F_{o,\,hkl}|$ and $|F_{c,\,hkl}|$ are the observed and calculated structure factor amplitudes.

[c] R_{free} is equivalent to R_{work} but calculated with reflections omitted from the refinement process (5% of reflections omitted).

[d] Percentage of total number of residues in the "favoured," "allowed," "additionally allowed," and "disallowed" regions, respectively, of the Ramachandran plot according to PROCHECK definitions (Laskowski et al., 1993).

Dimerization of NCAM 2 IgI–IgII

The IgI–II and IgI–III structures reveal one significant protein-protein interface with an area of ~980 $Å^2$ in the IgI–II structure with ten hydrogen bonds and six salt bridges in the interface (residues involved in dimerization can be seen in Figure 1). In the IgI–III structure the interface area is only ~620 $Å^2$, possibly due to a smaller angle between the molecules constituting the dimer than in the IgI–II dimer (113° versus 133°) (Figure 3A). The dimer interfaces obtained from the IgI-II and IgI-III structures, respectively, are shown in Figure 3B. Approximately 80% of the residues involved in this dimer interface are conserved between NCAM1 and OCAM (Figure 1), and the OCAM interface is very similar to that observed in the NCAM1 IgI–II and IgI–III structures (Colley, 2010; Kasper et al., 2000; Soroka et al., 2003). Analysis of the crystal packing interactions in the four other structures did not reveal any other significant interfaces.

To investigate the IgI–IgII dimerization in solution, gel filtration chromatography was applied. The protein eluted as one peak at an elution time corresponding to the dimeric form of the protein (Figure S3A). Moreover, OCAM IgI–III, comprising 291 amino acids, eluted as a protein with a higher molecular weight than OCAM IgIV–Fn3II, comprising 400 amino acids (Figure S3B), indicating that IgI–III dimerizes in solution. To further investigate the structure of OCAM IgI–III in solution, the protein was subjected to small-angle X-ray scattering (SAXS) analysis. The molecular weight of the solute was estimated to be 72 kDa, corresponding to the expected molecular weight of a dimer (69 kDa). The pairwise distance distribution function (P[r]) derived from the solution-scattering curve (Figure S4) indicates a maximal dimension of the protein dimer of 150 Å. This dimension is significantly larger than the maximal distances observed within the crystal structure of the IgI–III dimer (~130 Å). The modular buildup of the dimer is evident from the P(r), which

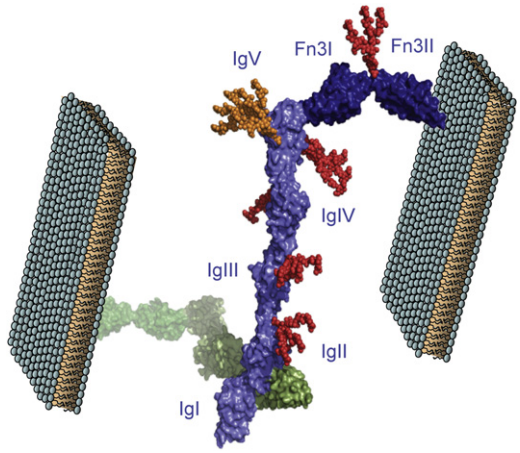

Figure 5. Structural Model of the Entire OCAM Ectodomain Built from the Overlapping IgI–II, IgII–III, IgIII–IV, and IgIV–Fn3II Structures
On the model, *N*-glycosylations are modeled as the complex sialylated fucosylated triantennary type. The glycosylation corresponding to the position of the polysialylation in NCAM is colored orange. The rest of the glycosylations are colored red. See also Figures S1 and S3.

clearly shows the presence of a typical distance around 20 Å, corresponding to the radius of gyration (Rg) of an Ig domain. An ab initio bead model can be fitted by the IgI–IgIII crystal structure in which the intermolecular angle (angle between molecules in the dimer) is opened an additional 28°.

Structural analysis of the dimerization site indicated that Leu27, Phe39, and Arg77 contribute significantly to the interaction interface. To verify the role of these amino acids, the following two double mutants were produced: Leu27Ser + Phe39Ser (IgI–IILF) and Phe39Ser + Arg77Glu (IgI–IIFR). Both proteins eluted as broad peaks, corresponding to combined monomeric and dimeric forms of the proteins, whereas the intact protein eluted as a single peak at elution time corresponding to the dimeric form (Figure S3A). Therefore, the introduced mutations partly disrupt the IgI–IgII dimer interface.

Structural Model of the Ectodomain

A model of the entire extracellular part of OCAM was built from overlapping IgI–II, IgII–III, IgIII–IV, and IgIV–Fn3II structures (Figure 5). The model represents a complete dimer of the OCAM ectodomain interpreted as a *trans*-interacting homodimer with a cell-to-cell distance of about 20 nm.

DISCUSSION

To understand the structural context for homophilic binding of Ig CAMs, we previously attempted to crystallize NCAM1 and L1 ectodomain fragments consisting of more than four domains, but these crystals only diffracted to low resolution (Kulahin et al., 2004, 2005a). In the present study we chose another strategy and crystallized several overlapping constructs of the OCAM ectodomain. This approach allowed the construction of a structural model of the entire ectodomain based on six overlapping structures of truncated versions of the protein. Altogether, the high consistency in tilt and twist angles (Figure 2A) in combination with the results of the molecular dynamics simulations support the notion that the average conformations of the various recombinant OCAM proteins resemble the conformations seen in the crystals. Consequently, a structural model of the entire OCAM ectodomain was assembled from the crystallized overlapping modular constructs. The model is shown in Figure 5. It consists of an essentially linear segment composed of the IgI–V domains, followed by bent hinges between the IgV and Fn3I domains and between the Fn3I and Fn3II domains. The tilt and twist angles in IgI–II and IgI–III are comparable to the angles observed in NCAM1 (Figure 2B) (Kasper et al., 2000; Soroka et al., 2003). Furthermore, the angles between IgI and IgII are also within the same range as the angles observed in the crystal structures of VCAM IgI–II (Wang et al., 1995) and the EC domains in N- and E-cadherin (Koch et al., 1999). These findings further support a model in which the entire OCAM IgI–V segment can adopt an essentially linear conformation, with variations of only 10°–15° in the hinges.

The bend between OCAM IgV and Fn3I in the IgIV–Fn3I structure is caused by a HEPES molecule bound in the hinge region, and the structure can represent one of several OCAM conformations. This is consistent with findings from electron microscopy that identified a hinge region around IgV in NCAM1 (Hall and Rutishauser, 1987). The bend between OCAM IgV and Fn3I is less pronounced in the OCAM IgIV–Fn3II structure. However, models of the entire ectodomain based on the IgIV–Fn3I structure (with a tilt angle of 98°) and the IgIV–Fn3II structure (with a tilt angle of 52°) result in approximately the same intercellular distances, and both models imply that the Ig domains can be positioned parallel with and in quite close proximity to the cell surface. The residues that interact with the HEPES molecule are conserved between NCAMs from several species (Figure S2) and may, therefore, form a regulatory binding site that is functionally important for all NCAMs.

The analysis of the IgIV–Fn3II structure did not reveal any interdomain interactions between the Fn3 domains, which together with the results from the molecular dynamics simulations indicate that the hinge region between these domains is one of the flexible regions in the OCAM ectodomain. This interpretation is supported by the structure of NCAM1 Fn3I–II, which also indicates that the link between the NCAM1 Fn3I and Fn3II is flexible (Carafoli et al., 2008).

Protein-protein interactions in crystals may represent biologically important interactions, and several publications have shown that biologically important adhesion interactions can be found in the crystalline phase, although they are not detected in solution (Freigang et al., 2000). A recent structure model of OCAM IgI suggested that this module exhibits domain swapping created by an interchange of the N-terminal A1 β strands (Rasmussen et al., 2008). However, in the present study, neither the IgI–II nor the IgI–III structure demonstrated any domain swapping between the IgI domains, and in the six OCAM structures presented in this study, the IgI–II dimerization was the only homophilic interaction observed in more than one crystal structure. This interface is composed of essentially three linear epitopes, formed by residues equivalent to residues forming the IgI–II dimer in NCAM1 (Figure 1). Five interface residues (Lys38, Phe39, Thr79, Tyr81, and Arg189) are conserved between NCAM1 and OCAM, suggesting that they play a primary

role as contributors to affinity. Conversely, the Thr41, Arg77, and Glu191 residues of OCAM may provide specificity for homophilic binding. These residues correspond to Leu40, Thr80, and Leu194 in NCAM1, and these differences in the protein sequence may explain why NCAM1 and OCAM do not bind each other (Yoshihara et al., 1997). The angles between the molecules comprising the NCAM1 and OCAM dimers (Figure 3A) suggest plasticity of the dimer interface. This is especially pronounced in OCAM, where the intermolecular angles derived from the IgI–II and IgI–III structures differ by 20°. The difference in the angle can probably be explained by different crystal packing of the proteins. Solution-scattering experiments suggest even more pronounced plasticity of the dimer interface (Figure S4). Molecular dynamics simulations indicate that the IgI–II hinge is one of the most flexible ectodomain regions, further supporting the dependence of the intermolecular angle on the conformational restrictions on the protein (crystal versus solution conformation). The flexibility of the IgI–II hinge might be necessary for conformational adaptation during OCAM dimerization and is probably reduced after the dimer formation, resulting in a linear conformation of the region.

NCAM1-mediated homophilic cell adhesion has been the topic of several studies (reviewed in Soroka et al., 2010). The first models, based on cell or microsphere aggregation techniques, suggested that the IgIII domain mediated the *trans*-homophilic interaction (Rao et al., 1992). Later, an IgI-IgII interaction was detected by surface plasmon resonance (Kiselyov et al., 1997), and this gave rise to a model in which *trans*-homophilic binding was mediated by IgI–II dimerization. The most recent model is based on the crystal structure of NCAM1 IgI–III (Soroka et al., 2003). Interestingly, this model interprets the IgI–IgII interaction as a *cis*-interaction, whereas homophilic NCAM1 *trans*-interactions are mediated by zipper-like interactions among IgI–IgIII, IgII–IgIII, and IgII–IgII (Figure S1). In contrast the results presented in this study clearly suggest that in OCAM the IgI–IgII interaction represents a *trans*-interaction (Figure 5), whereas no homophilic *cis*-interactions were identified.

In conclusion the presented structural model of OCAM suggests that the molecule forms *trans*-homophilic dimers through reciprocal IgI-IgII interactions, and that the Ig domains form a linear segment positioned parallel to the cell surface, followed by bends in the more membrane-proximal part of the molecule. Moreover, the majority of the flexibility of the structure seems to be restricted to the membrane-proximal hinges of the molecule, and to the IgI-IgII dimerization interface. The spatial arrangement may facilitate heterophilic interactions between the OCAM ectodomain and unidentified counter-receptors. Whereas little is known about OCAM interactions, NCAM1 is known to form numerous extracellular heterophilic interactions, including interactions between the NCAM1 Fn3 domains and the fibroblast growth factor receptor and interactions with several extracellular matrix molecules (Nielsen et al., 2010; Walmod et al., 2004).

The model of the OCAM ectodomain described here implies that homophilic OCAM interactions lead to an intercellular distance of about 20 nm. This intercellular distance is comparable to the 14 nm intercellular distance recently reported for the *trans*-heterophilic SIRPα-CD47 interaction (Hatherley et al., 2009). In support of these models, such distances between cell membranes are observed in chemical synapses (Hormuzdi et al., 2004).

EXPERIMENTAL PROCEDURES

Protein Cloning and Expression

Constructs encoding recombinant protein were prepared using polymerase chain reaction amplification of human *NCAM2* cDNA (Ensembl Gene ID ENSG00000154654; RZPD, Germany) for subcloning into the ClaI/NotI sites of the pPICZα C plasmid (Invitrogen). All recombinant proteins consist of two N-terminal residues (Ser and Met) remaining from the cloning procedure, followed by amino acids from various recombinant human OCAM proteins (Swiss-Prot code O15394) and six C-terminal histidine residues. The IgI–II construct comprises amino acids 19–218, IgII–III amino acids 115–301, IgI–III amino acids 19–301, IgIII–IV amino acids 209–400, IgIV–Fn3I amino acids 302–593, and IgIV–Fn3II amino acids 302–693. Two double mutants of IgI–II (IgI–IILF and IgI–IIFR) were produced using a Phusion™ Site-Directed Mutagenesis Kit (Finnzymes). Mutations Leu27Ser and Phe39Ser and mutations Phe39Ser and Arg77Glu were introduced into the OCAM IgI–IILF and OCAM IgI–IIFR mutants, respectively. All constructs were verified by DNA sequencing. The recombinant plasmids were linearized with SacI enzyme and used for transformation of the *Pichia pastoris* strain KM71H (Invitrogen). Transformation and selection were performed by the protocol supplied by the manufacturer. A preinduction culture was grown for 48 hr in BMGH medium before transfer and continued growth and induction in BMMH medium for 24 hr. The secreted proteins were purified using Ni-NTA (QIAGEN) affinity chromatography. All proteins were deglycosylated using Endo Hf (New England Biolabs). As a final purification step, gel filtration chromatography was performed either in phosphate-buffered saline (PBS; Sigma; for SAXS experiments and analytical gel filtration chromatography) or 10 mM HEPES (Sigma) (pH 7.4), 20 mM NaCl (Sigma; for X-ray crystallography experiments). All protein constructs were concentrated to 3–8 mg/ml using Amicon Centrifugal Filter Units (Millipore).

Gel Filtration Chromatography

Gel filtration chromatography was performed with a HiLoad 16/60 Superdex 200 prep grade column (GE Healthcare) connected to an Äkta FPLC system (GE Healthcare). The flow rate was 1 ml/min, and the temperature was 5°C–6°C in all experiments. The column was equilibrated with PBS (pH 7.4) or 10 mM HEPES (pH 7.4), 20 mM NaCl. The column was calibrated in PBS (Figure S2C). The calibration set (GE Healthcare) included blue dextran 2000 (~2000 kDa), thyroglobulin (669 kDa), ferritin (444 kDa), aldolase (158 kDa), conalbumin (75 kDa), ovalbumin (43 kDa), and chymotrypsinogen A (25 kDa). Two milliliters of protein were injected onto the column.

Crystallization and Crystal Structure Determinations

Crystallization was achieved by hanging-drop experiments by mixing 1 μl protein and 1 μl reservoir solution (30% PEG-4000, 0.2 M sodium acetate trihydrate, 0.1 M tris hydrochloride [pH 8.5], for IgI–II; 30% PEG-4000, 0.2 M lithium sulfate, 0.1 M tris hydrochloride [pH 8.5], for IgII–III; 25% PEG-6000, 0.1 M HEPES [pH 7.0], for IgIII–IV; 4% PEG-3350, 0.02 M calcium chloride, 0.1 M citric acid [pH 4.5], for IgI–III; 10% PEG-3350, 0.1 M ammonium phosphate, 0.01 M trimethylamine hydrochloride for IgIV–Fn3I; and 14% PEG-10000, 0.2 M calcium acetate, 0.1 M HEPES [pH 6.5], for IgIV–Fn3II). All chemicals were purchased from Sigma-Aldrich. Diffraction data on all six truncations of OCAM were collected at 100 K. Details of data collection and processing are presented in Table 1. The structures were determined by the molecular replacement method using the program PHASER (Storoni et al., 2004). Details on the models used for the molecular replacement method are provided in the Supplemental Experimental Procedures. Model building was performed using the program ARP/wARP (Perrakis et al., 1999) and manual correction using the program COOT (Emsley and Cowtan, 2004). The program PHENIX (Adams et al., 2002) was used for refinement, and the quality of the final structures was examined using PROCHECK (Laskowski et al., 1993). Analysis of binding interfaces was performed using PISA server (http://www.ebi.ac.uk/msd-srv/prot_int/pistart.html, accessed November 28, 2009).

Molecular Dynamics

Molecular dynamics simulations were performed with the Amber software suite, version 8 (Case et al., 2005). Parameters were from the Amber99 force field (Wang et al., 2000) for all molecules, with the exception that the NAG and HEPES molecules in model IgIV–Fn3I used the parameters from the gaff force field (Wang et al., 2004).

The complexes were solvated in octahedral boxes of water molecules, extending at least 8 Å outside the protein. Hydrogen atoms and water molecules were added using the LEaP module in Amber, assuming that all Asp and Glu residues were negatively charged and that the Lys and Arg residues were positively charged.

The solvent and hydrogen atoms were relaxed by a short molecular mechanics minimization (100 steps), followed by 20 ps molecular dynamics simulation. After relaxation, the entire system was equilibrated by 50 ps of constant pressure simulations, followed by 200 ps of constant volume simulations. Finally, a production simulation of 10 ns was performed for each system. All simulations were performed using a time step of 2 fs. Additional details are provided in the Supplemental Experimental Procedures.

Solution SAXS

SAXS data collection was performed at beamline I711 (MAXlab, Lund, Sweden) in the momentum transfer range $0.010 < s < 0.325$ Å^{-1} ($s = 4\pi \sin\theta/\lambda$, where θ is half the scattering angle) using a wavelength of 1.05 Å and a MAR165 CCD detector. The sample exposure time was 10 min. Buffers were measured before and after sample exposure and averaged before background subtraction. Repeated exposure did not reveal any radiation damage. BioXTAS RAW (Toft et al., 2008) software was used for radial averaging and background subtraction. The average molecular mass of the protein was estimated from the extrapolated forward scattering I(0) by using a reference solution of bovine serum albumin. The data were fitted to theoretical scattering curves of relevant structures using the program CRYSOL (Svergun et al., 1995). The indirect Fourier transform program GNOM (Svergun, 1992) calculated the P(r) and estimated the average Rg and the maximal distance (D_{max}) within the scattering protein. The program DAMMIF (Franke and Svergun, 2009) was applied to calculate ab initio bead models, representing the overall solution conformation. Starting parameters for the modeling was a sphere with a diameter of 160 Å, using standard settings. P2 symmetry was evident from the initial run, and 20 models were correspondingly calculated by applying symmetry. These models were averaged and filtered to the final model in the program DAMAVER (Volkov and Svergun, 2003).

ACCESSION NUMBERS

Coordinates have been deposited in the RCSB Protein Data Bank with accession codes 2WIM, 2V5T, 2JLL, 2XYC, 2XY2, and 2XY1.

SUPPLEMENTAL INFORMATION

Supplemental Information includes Supplemental Experimental Procedures, four figures, and two tables and can be found with this article online at doi:10.1016/j.str.2010.12.014.

ACKNOWLEDGMENTS

We thank Carlsbergfondet, Augustinus Fonden, Beckett-Fonden, and the Danish synchrotron user organization DANSCATT for financial support. The authors declare that they have no conflict of interest.

Received: May 25, 2010
Revised: November 10, 2010
Accepted: December 12, 2010
Published: February 8, 2011

REFERENCES

Adams, P.D., Grosse-Kunstleve, R.W., Hung, L.W., Ioerger, T.R., McCoy, A.J., Moriarty, N.W., Read, R.J., Sacchettini, J.C., Sauter, N.K., and Terwilliger, T.C. (2002). PHENIX: building new software for automated crystallographic structure determination. Acta Crystallogr. D Biol. Crystallogr. *58*, 1948–1954.

Alenius, M., and Bohm, S. (1997). Identification of a novel neural cell adhesion molecule-related gene with a potential role in selective axonal projection. J. Biol. Chem. *272*, 26083–26086.

Bork, P., Downing, A.K., Kieffer, B., and Campbell, I.D. (1996). Structure and distribution of modules in extracellular proteins. Q. Rev. Biophys. *29*, 119–167.

Carafoli, F., Saffell, J.L., and Hohenester, E. (2008). Structure of the tandem fibronectin type 3 domains of neural cell adhesion molecule. J. Mol. Biol. *377*, 524–534.

Case, D.A., Cheatham, T.E., 3rd, Darden, T., Gohlke, H., Luo, R., Merz, K.M., Jr., Onufriev, A., Simmerling, C., Wang, B., and Woods, R.J. (2005). The Amber biomolecular simulation programs. J. Comput. Chem. *26*, 1668–1688.

Colley, K.J. (2010). Structural basis for the polysialylation of the neural cell adhesion molecule. Adv. Exp. Med. Biol. *663*, 111–126.

Edwards, S., Campbell, C., Flohr, P., Shipley, J., Giddings, I., Te-Poele, R., Dodson, A., Foster, C., Clark, J., Jhavar, S., et al. (2005). Expression analysis onto microarrays of randomly selected cDNA clones highlights HOXB13 as a marker of human prostate cancer. Br. J. Cancer *92*, 376–381.

Emsley, P., and Cowtan, K. (2004). Coot: model-building tools for molecular graphics. Acta Crystallogr. D Biol. Crystallogr. *60*, 2126–2132.

Franke, D., and Svergun, D.I. (2009). DAMMIF, a program for rapid ab-initio shape determination in small-angle scattering. J. Appl. Crystallogr. *42*, 342–346.

Freigang, J., Proba, K., Leder, L., Diederichs, K., Sonderegger, P., and Welte, W. (2000). The crystal structure of the ligand binding module of axonin-1/TAG-1 suggests a zipper mechanism for neural cell adhesion. Cell *101*, 425–433.

Hall, A.K., and Rutishauser, U. (1987). Visualization of neural cell adhesion molecule by electron microscopy. J. Cell Biol. *104*, 1579–1586.

Hamlin, J.A., Fang, H., and Schwob, J.E. (2004). Differential expression of the mammalian homologue of fasciclin II during olfactory development in vivo and in vitro. J. Comp. Neurol. *474*, 438–452.

Haspel, J., and Grumet, M. (2003). The L1CAM extracellular region: a multi-domain protein with modular and cooperative binding modes. Front. Biosci. *8*, s1210–s1225.

Hatherley, D., Graham, S.C., Harlos, K., Stuart, D.I., and Barclay, A.N. (2009). Structure of signal-regulatory protein alpha: a link to antigen receptor evolution. J. Biol. Chem. *284*, 26613–26619.

Holm, L., Kaariainen, S., Rosenstrom, P., and Schenkel, A. (2008). Searching protein structure databases with DaliLite v.3. Bioinformatics *24*, 2780–2781.

Hormuzdi, S.G., Filippov, M.A., Mitropoulou, G., Monyer, H., and Bruzzone, R. (2004). Electrical synapses: a dynamic signaling system that shapes the activity of neuronal networks. Biochim. Biophys. Acta *1662*, 113–137.

Ichinohe, N., Yoshihara, Y., Hashikawa, T., and Rockland, K.S. (2003). Developmental study of dendritic bundles in layer 1 of the rat granular retrosplenial cortex with special reference to a cell adhesion molecule, OCAM. Eur. J. Neurosci. *18*, 1764–1774.

Juliano, R.L. (2002). Signal transduction by cell adhesion receptors and the cytoskeleton: functions of integrins, cadherins, selectins, and immunoglobulin-superfamily members. Annu. Rev. Pharmacol. Toxicol. *42*, 283–323.

Kabsch, W., and Sander, C. (1983). Dictionary of protein secondary structure: pattern recognition of hydrogen-bonded and geometrical features. Biopolymers *22*, 2577–2637.

Kasper, C., Rasmussen, H., Kastrup, J.S., Ikemizu, S., Jones, E.Y., Berezin, V., Bock, E., and Larsen, I.K. (2000). Structural basis of cell-cell adhesion by NCAM. Nat. Struct. Biol. *7*, 389–393.

Kiselyov, V.V., Berezin, V., Maar, T.E., Soroka, V., Edvardsen, K., Schousboe, A., and Bock, E. (1997). The first immunoglobulin-like neural cell adhesion molecule (NCAM) domain is involved in double-reciprocal interaction with the second immunoglobulin-like NCAM domain and in heparin binding. J. Biol. Chem. *272*, 10125–10134.

Kiselyov, V.V., Skladchikova, G., Hinsby, A.M., Jensen, P.H., Kulahin, N., Soroka, V., Pedersen, N., Tsetlin, V., Poulsen, F.M., Berezin, V., and Bock,

E. (2003). Structural basis for a direct interaction between FGFR1 and NCAM and evidence for a regulatory role of ATP. Structure *11*, 691–701.

Koch, A.W., Bozic, D., Pertz, O., and Engel, J. (1999). Homophilic adhesion by cadherins. Curr. Opin. Struct. Biol. *9*, 275–281.

Kulahin, N., and Walmod, P.S. (2010). The neural cell adhesion molecule NCAM2/OCAM/RNCAM, a close relative to NCAM. Adv. Exp. Med. Biol. *663*, 403–420.

Kulahin, N., Kasper, C., Gajhede, M., Berezin, V., Bock, E., and Kastrup, J.S. (2004). Expression, crystallization and preliminary X-ray analysis of extracellular modules of the neural cell-adhesion molecules NCAM and L1. Acta Crystallogr. D Biol. Crystallogr. *60*, 591–593.

Kulahin, N., Kasper, C., Kristensen, O., Kastrup, J.S., Berezin, V., Bock, E., and Gajhede, M. (2005a). Expression, crystallization and preliminary X-ray analysis of the extracellular Ig modules I-IV and F3 modules I-III of the neural cell-adhesion molecule L1. Acta Crystallogr. Sect. F Struct. Biol. Cryst. Commun. *61*, 858–860.

Kulahin, N., Rudenko, O., Kiselyov, V., Poulsen, F.M., Berezin, V., and Bock, E. (2005b). Modulation of the homophilic interaction between the first and second Ig modules of neural cell adhesion molecule by heparin. J. Neurochem. *95*, 46–55.

Laskowski, R.A., Moss, D.S., and Thornton, J.M. (1993). Main-chain bond lengths and bond angles in protein structures. J. Mol. Biol. *231*, 1049–1067.

Mendiratta, S.S., Sekulic, N., Hernandez-Guzman, F.G., Close, B.E., Lavie, A., and Colley, K.J. (2006). A novel alpha-helix in the first fibronectin type III repeat of the neural cell adhesion molecule is critical for N-glycan polysialylation. J. Biol. Chem. *281*, 36052–36059.

Molloy, C.A., Keddache, M., and Martin, L.J. (2005). Evidence for linkage on 21q and 7q in a subset of autism characterized by developmental regression. Mol. Psychiatry *10*, 741–746.

Mortl, M., Sonderegger, P., Diederichs, K., and Welte, W. (2007). The crystal structure of the ligand-binding module of human TAG-1 suggests a new mode of homophilic interaction. Protein Sci. *16*, 2174–2183.

Nielsen, J., Kulahin, N., and Walmod, P.S. (2010). Extracellular protein interactions mediated by the neural cell adhesion molecule, NCAM: heterophilic interactions between NCAM and cell adhesion molecules, extracellular matrix proteins, and viruses. Adv. Exp. Med. Biol. *663*, 23–53.

Owczarek, S.E., Kristiansen, L.V., Hortsch, M., and Walmod, P.S. (2009). Cell adhesion molecules of the NCAM family and their role at synapses. In The Sticky Synapse, M. Hortsch and H. Umemori, eds. (New York: Springer), pp. 265–299.

Paoloni-Giacobino, A., Chen, H., and Antonarakis, S.E. (1997). Cloning of a novel human neural cell adhesion molecule gene (NCAM2) that maps to chromosome region 21q21 and is potentially involved in Down syndrome. Genomics *43*, 43–51.

Perrakis, A., Morris, R., and Lamzin, V.S. (1999). Automated protein model building combined with iterative structure refinement. Nat. Struct. Biol. *6*, 458–463.

Prota, A.E., Campbell, J.A., Schelling, P., Forrest, J.C., Watson, M.J., Peters, T.R., Aurrand-Lions, M., Imhof, B.A., Dermody, T.S., and Stehle, T. (2003). Crystal structure of human junctional adhesion molecule 1: implications for reovirus binding. Proc. Natl. Acad. Sci. USA *100*, 5366–5371.

Rao, Y., Wu, X.F., Gariepy, J., Rutishauser, U., and Siu, C.H. (1992). Identification of a peptide sequence involved in homophilic binding in the neural cell adhesion molecule NCAM. J. Cell Biol. *118*, 937–949.

Rasmussen, K.K., Kulahin, N., Kristensen, O., Poulsen, J.C., Sigurskjold, B.W., Kastrup, J.S., Berezin, V., Bock, E., Walmod, P.S., and Gajhede, M. (2008). Crystal structure of the Ig1 domain of the neural cell adhesion molecule NCAM2 displays domain swapping. J. Mol. Biol. *382*, 1113–1120.

Raveh, S., Gavert, N., and Ben-Ze'ev, A. (2009). L. cell adhesion molecule (L1CAM) in invasive tumors. Cancer Lett. *282*, 137–145.

Reyes, A.A., Akeson, R., Brezina, L., and Cole, G.J. (1990). Structural requirements for neural cell adhesion molecule-heparin interaction. Cell Regul. *1*, 567–576.

Rice, G.P., Hartung, H.P., and Calabresi, P.A. (2005). Anti-alpha4 integrin therapy for multiple sclerosis: mechanisms and rationale. Neurology *64*, 1336–1342.

Sawaya, M.R., Wojtowicz, W.M., Andre, I., Qian, B., Wu, W., Baker, D., Eisenberg, D., and Zipursky, S.L. (2008). A double S shape provides the structural basis for the extraordinary binding specificity of Dscam isoforms. Cell *134*, 1007–1018.

Shapiro, L., Doyle, J.P., Hensley, P., Colman, D.R., and Hendrickson, W.A. (1996). Crystal structure of the extracellular domain from P0, the major structural protein of peripheral nerve myelin. Neuron *17*, 435–449.

Shapiro, L., Love, J., and Colman, D.R. (2007). Adhesion molecules in the nervous system: structural insights into function and diversity. Annu. Rev. Neurosci. *30*, 451–474.

Soroka, V., Kasper, C., and Poulsen, F.M. (2010). Structural biology of NCAM. Adv. Exp. Med. Biol. *663*, 3–22.

Soroka, V., Kolkova, K., Kastrup, J.S., Diederichs, K., Breed, J., Kiselyov, V.V., Poulsen, F.M., Larsen, I.K., Welte, W., Berezin, V., et al. (2003). Structure and interactions of NCAM Ig1-2-3 suggest a novel zipper mechanism for homophilic adhesion. Structure *11*, 1291–1301.

Storoni, L.C., McCoy, A.J., and Read, R.J. (2004). Likelihood-enhanced fast rotation functions. Acta Crystallogr. D Biol. Crystallogr. *60*, 432–438.

Svergun, D. (1992). Determination of the regularization parameter in indirect-transform methods using perceptual criteria. J. Appl. Crystallogr. *25*, 495–503.

Svergun, D., Barberato, C., and Koch, M.H.J. (1995). CRYSOL— a program to evaluate X-ray solution scattering of biological macromolecules from atomic coordinates. J. Appl. Crystallogr. *28*, 768–773.

Toft, K.N., Vestergaard, B., Nielsen, S.S., Snakenborg, D., Jeppesen, M.G., Jacobsen, J.K., Arleth, L., and Kutter, J.P. (2008). High-throughput small angle X-ray scattering from proteins in solution using a microfluidic front-end. Anal. Chem. *80*, 3648–3654.

Volkov, V.V., and Svergun, D.I. (2003). Uniqueness of ab initio shape determination in small-angle scattering. J. Appl. Crystallogr. *36*, 860–864.

Walmod, P.S., Kolkova, K., Berezin, V., and Bock, E. (2004). Zippers make signals: NCAM-mediated molecular interactions and signal transduction. Neurochem. Res. *29*, 2015–2035.

Wang, J., and Springer, T.A. (1998). Structural specializations of immunoglobulin superfamily members for adhesion to integrins and viruses. Immunol. Rev. *163*, 197–215.

Wang, J.H., Pepinsky, R.B., Stehle, T., Liu, J.H., Karpusas, M., Browning, B., and Osborn, L. (1995). The crystal structure of an N-terminal two-domain fragment of vascular cell adhesion molecule 1 (VCAM-1): a cyclic peptide based on the domain 1 C-D loop can inhibit VCAM-1-alpha 4 integrin interaction. Proc. Natl. Acad. Sci. USA *92*, 5714–5718.

Wang, J., Cieplak, P., and Kollman, P. (2000). How well does a restrained electrostatic potential (RESP) model perform in calculating conformational energies of organic and biological molecules? J. Comput. Chem. *21*, 1049–1074.

Wang, J., Wolf, R.M., Caldwell, J.W., Kollman, P.A., and Case, D.A. (2004). Development and testing of a general amber force field. J. Comput. Chem. *25*, 1157–1174.

Xu, L.L., Su, Y.P., Labiche, R., Segawa, T., Shanmugam, N., McLeod, D.G., Moul, J.W., and Srivastava, S. (2001). Quantitative expression profile of androgen-regulated genes in prostate cancer cells and identification of prostate-specific genes. Int. J. Cancer *92*, 322–328.

Yoshihara, Y., Kawasaki, M., Tamada, A., Fujita, H., Hayashi, H., Kagamiyama, H., and Mori, K. (1997). OCAM: a new member of the neural cell adhesion molecule family related to zone-to-zone projection of olfactory and vomeronasal axons. J. Neurosci. *17*, 5830–5842.